A Letters Journal Exploring the Frontiers of Physics

March 2009

EPL, **85** (2009) 68001
doi: 10.1209/0295-5075/85/68001

www.epljournal.org

Intermodulation and parametric amplification in a superconducting stripline resonator integrated with a dc-SQUID

B. Abdo[1(a)], O. Suchoi[1], E. Segev[1], O. Shtempluck[1], M. Blencowe[2] and E. Buks[1]

[1] *Department of Electrical Engineering, Technion - Haifa 32000, Israel*
[2] *Department of Physics and Astronomy, Dartmouth College - Hanover, NH 03755, USA*

received 17 November 2008; accepted in final form 23 February 2009
published online 31 March 2009

PACS 85.25.Dq – Superconducting quantum interference devices (SQUIDs)
PACS 84.40.Dc – Microwave circuits
PACS 05.45.-a – Nonlinear dynamics and chaos

Abstract – We utilize a superconducting stripline resonator containing a dc-SQUID as a strong intermodulation amplifier exhibiting a signal gain of 24 dB and a phase modulation of 30 dB. Studying the system response in the time domain near the intermodulation amplification threshold reveals a unique noise-induced spikes behavior. We account for this response qualitatively via solving numerically the equations of motion for the integrated system. Furthermore, employing this device as a parametric amplifier yields an abrupt rise of 38 dB in the generated side-band signal.

The field of solid-state qubits and quantum information processing has received considerable attention during the past decade [1–4] and has successfully demonstrated several milestone results to date [5–11]. However, one of the fundamental challenges hindering this emerging field is noise interference, which either screens the output signal or leads to quantum state decoherence [5,6,12–15]. Hence, this may explain to some extent the renewed interest exhibited recently by the quantum measurement community in the field of parametric amplifiers [16–21]. This interest is driven essentially by two important properties of these amplifiers: 1) their capability to amplify very weak coherent signals; 2) their ability to squeeze noise below the equilibrium level by means of employing a homodyne setup and phase control. These properties are expected to be highly beneficial to the area of quantum communication [22,23] and to the generation of quantum squeezed states [16,17,24,25]. Additional interest in these high-gain parametric amplifiers arises from the large body of theoretical work predicting photon-generation from vacuum via the dynamical Casimir effect [26,27], which can be achieved by employing an appropriate parametric excitation mechanism [28,29].

In this present work we study a superconducting stripline microwave resonator integrated with a dc-SQUID [30–32]. The paper is mainly devoted to a novel amplification mechanism in which the relatively large nonlinear inductance of the dc-SQUID is exploited to achieve large gain in an intermodulation (IM) configuration. We provide theoretical evidence to support our hypothesis that the underlying mechanism responsible for the large observed gain is the metastability of the dc-SQUID. In addition, at the end of the paper we demonstrate another amplification mechanism, in which the dependence of the dc-SQUID inductance on the external magnetic field is exploited to achieve parametric amplification [20].

The device (see fig. 1(a)) is implemented on a high-resistivity 34 mm × 30 mm × 0.5 mm silicon wafer coated with a 100 nm thick layer of SiN. As a preliminary step, thick gold pads (300 nm) are evaporated at the periphery of the wafer. Following a stage of e-beam lithography, a two-angle shadow evaporation of aluminium [33] —with an intermediate stage of oxidation— realizes both the resonator and the two $Al/AlO_x/Al$ Josephson junctions comprising the dc-SQUID. The total thickness of the aluminium evaporated is 80 nm (40 nm at each angle).

In general, IM generation is often associated with the occurrence of nonlinear effects in the resonance curves of a superconducting resonator [34–38]. In fig. 2 we show a transmission measurement of the resonator response, obtained using a vector network analyzer at the resonance while sweeping the frequency upwards. The measured resonance resides at $f_0 = 8.219$ GHz which corresponds to

(a) E-mail: baleegh@tx.technion.ac.il

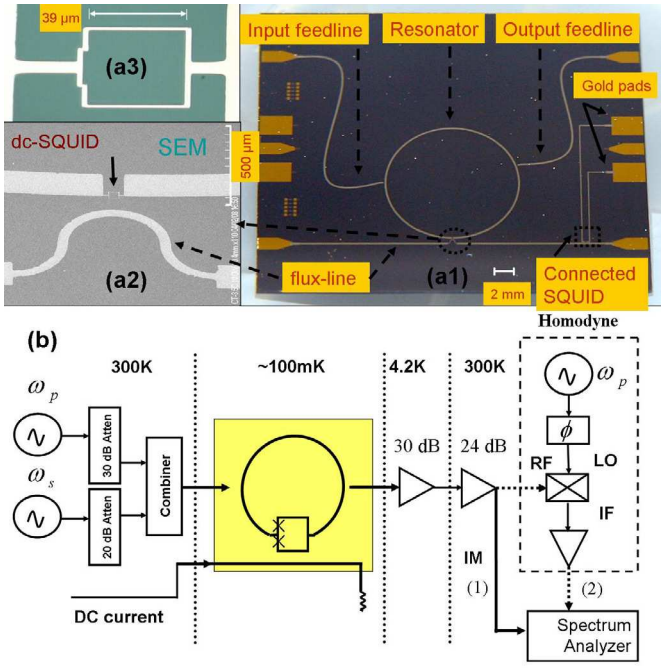

Fig. 1: (Color online) The device and IM setup. (a1) A photograph of the device consisting of a circular resonator with a circumference of 36.4 mm and a linewidth of 150 μm, a dc-SQUID integrated into the resonator and a flux line employed for driving rf-power and flux-biasing the dc-SQUID. The connected SQUID at the periphery of the wafer is employed for device characterization and dc measurements. (a2) An electron micrograph displaying the dc-SQUID incorporated in the resonator and the adjacent flux line. The area of the dc-SQUID fabricated is 39 μm $\times$39 μm, while the area of each junction is about 0.25 μm^2. The self-inductance of the dc-SQUID loop is $L_s = 1.3 \cdot 10^{-10}$ H and its total critical Josephson current is about $2I_c = 28\,\mu$A. (a3) A zoom-in optical-microscope image of the SQUID. (b) A basic IM setup. The pump and the signal designated by their angular frequency ω_p and ω_s, respectively, are combined by a power combiner and fed to the resonator. The field at the output is amplified using two amplification stages and measured using a spectrum analyzer (path 1). A dc current was applied to the flux line in order to flux-bias the dc-SQUID. Path (2) at the output corresponds to a homodyne setup employed in measuring IM.

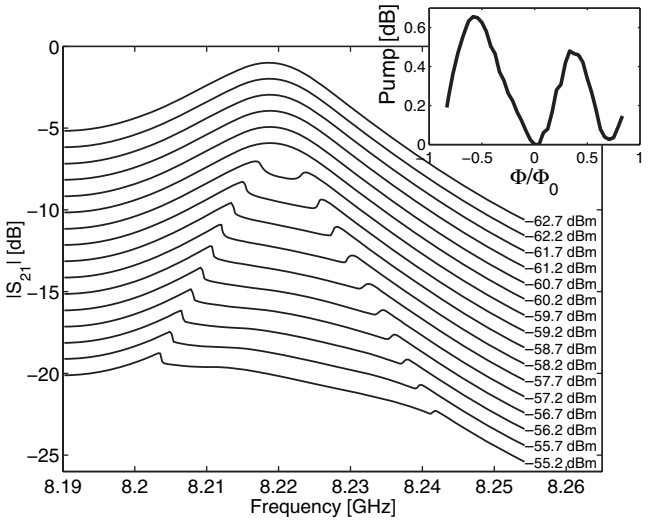

Fig. 2: Transmission response curves of the resonator at its third resonance (8.219 GHz) as a function of input power and frequency (the frequency was swept upwards). The resonance curves exhibit nonlinear effects at $P_p \gtrsim P_c$. The loaded quality factor for this resonance in the linear regime is 350. The resonance curves corresponding to different input powers were offset by a 1 dB for clarity. The inset exhibits the relative change in the transmitted pump signal *vs.* the applied magnetic flux threading the dc-SQUID loop during an IM measurement. The measurement was taken at a fixed input pump power at the vicinity of P_c. The flux modulation is relative to zero-flux bias and was measured while sweeping the flux upwards.

the third resonance mode of the resonator having an anti-node of the rf-current waveform at the dc-SQUID position. Similar nonlinear effects in the transmission response have been measured at the first mode ($\simeq 2.766$ GHz) as well.

As can be seen in the figure, at excitation powers P_p below $P_c = -60.3$ dBm (at which nonlinear effects emerge) the resonance curve is linear and Lorentzian. As the input power is increased, abrupt jumps appear at both sides of the resonance. In addition, as one continues to increase the input power the resonance curves become shallower, broader and less symmetrical. Such power dependency can be attributed to the nonlinearity of the dc-SQUID inside the resonator which increases considerably as the amplitude of the driving current becomes comparable to the critical current.

The basic IM scheme used is schematically depicted in fig. 1(b). The input field of the resonator is composed of two sinusoidal fields generated by external microwave synthesizers and superimposed using a power combiner. The applied signals have unequal amplitudes. One, referred to as the pump, is an intense sinusoidal field with frequency f_p, whereas the other, referred to as the signal, is a small amplitude sinusoidal field with frequency $f_p + \delta$, where δ represents the frequency offset between the two signals. Due to the presence of a nonlinear element such as the dc-SQUID integrated into the resonator, frequency mixing between the pump and the signal yields an output idler field at frequency $f_p - \delta$. Thus the output field of the resonator, measured by a spectrum analyzer, consists mainly of three spectral components, the transmitted pump, the transmitted signal and the generated idler. The IM amplification in the signal, idler and the noise is obtained, as shown herein, by driving the dc-SQUID to its onset of instability via tuning the pump power. In the inset of fig. 2 we show how the device response changes during IM with respect to the flux degree of freedom at a constant pump power. Maximum IM amplification is attained near half-flux-quantum points.

In fig. 3 we show a typical IM measurement result. In this measurement the pump was tuned to the resonance

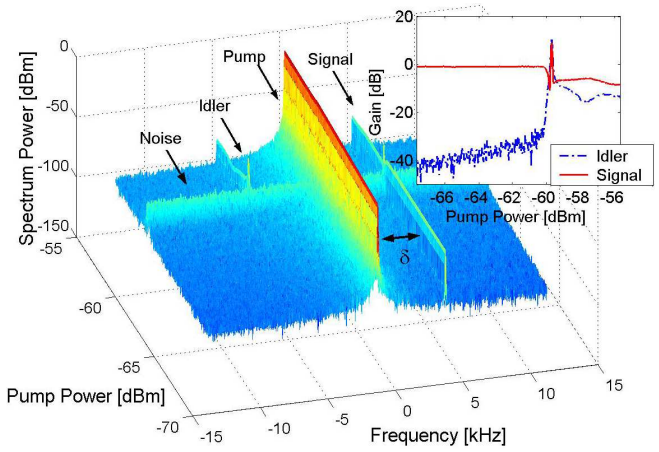

Fig. 3: (Color online) A spectrum power measured by a spectrum analyzer during IM operation as a function of increasing pump power while applying external flux $\Phi \simeq \Phi_0/4$, signal power $P_s = -110\,\mathrm{dBm}$, and frequency offset $\delta = 5\,\mathrm{kHz}$. The spectrum taken at a constant frequency span around f_p was shifted to dc for clarity. At the vicinity of P_c the system exhibits a large amplification. A cross-section of the measurement taken along the pump power axis is shown in the inset. The red line (solid line) and the blue line (dashdot line) exhibit the corresponding gain factors of the transmitted signal and the idler, respectively.

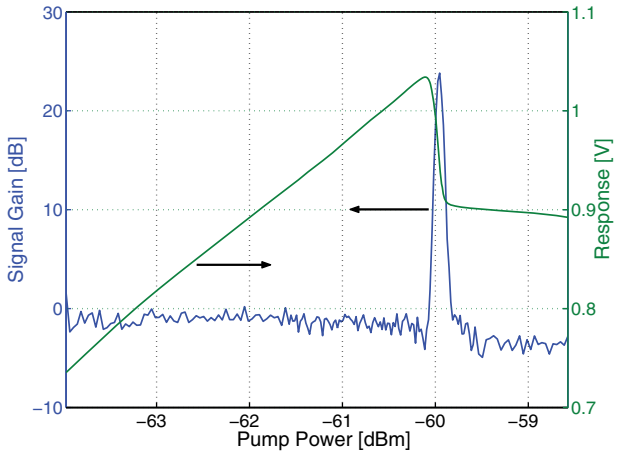

Fig. 4: (Color online) A signal gain (blue line) measured as a function of increasing pump power. The measurement was taken using a homodyne scheme. The signal displays a gain of about 24 dB at P_c. The corresponding dc component of the homodyne detector output (green line) was measured simultaneously using a voltage meter connected in parallel to the spectrum analyzer. In this measurement $\Phi \simeq \Phi_0/2$, $P_s = -110\,\mathrm{dBm}$, $\delta = 5\,\mathrm{kHz}$.

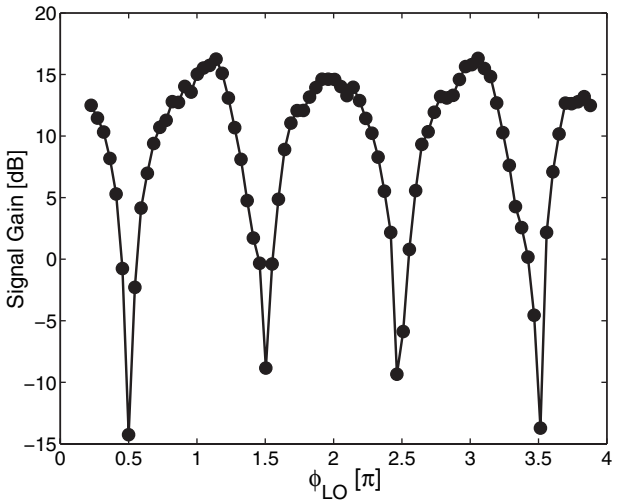

Fig. 5: A periodic dependence of the signal gain on the LO phase difference at the vicinity of P_c. The signal exhibits a large amplification and de-amplification at integer and half-integer multiples of π, respectively. The phase modulation dependency shows up to 30 dB peak-to-peak amplitude. In this measurement Φ, P_s and δ are the same as in the caption of fig. 4.

frequency $f_p = 8.219\,\mathrm{GHz}$. The signal power P_s was set to $-110\,\mathrm{dBm}$, and its frequency offset δ to 5 kHz. As the pump power injected into the resonator is increased, the nonlinearity of the dc-SQUID increases and consequently the frequency mixing between the pump and the signal increases as well. At about P_c the dc-SQUID reaches a critical point at which the idler, the signal and also the noise floor level (within the frequency bandwidth) undergo a large simultaneous amplification. The idler gain measured is 12 dB (see inset of fig. 3), where the signal/idler gain is defined as the ratio between the signal/idler power at the output feedline and the signal power at the input feedline. To this end, the losses and amplifications of the elements along each direction were calibrated with an uncertainty of ± 1 dB.

In order to show that this IM amplifier is also phase sensitive we applied a standard homodyne detection scheme as schematically depicted in fig. 1 (see path (2)), in which the phase difference between the pump and the local oscillator (LO) at the output —having the same frequency— can be varied. In such a scheme the pump is down-converted to dc, whereas both signal and idler are down-converted to the same frequency δ. The largest amplification is obtained when the LO phase (ϕ_{LO}) is adjusted such that the signal and idler tones constructively interfere. Shifting ϕ_{LO} by $\pi/2$ from the point of largest amplification results in destructive interference, which in turn leads to the largest de-amplification [16,17,24].

The IM measurement results, obtained using the homodyne setup while flux-biasing the dc-SQUID with about half-flux-quantum, are shown in figs. 4 and 5. Figure 4 exhibits the signal gain (blue line) *vs.* increasing applied pump power. As can be seen from the figure the signal gain assumes a peak of 24 dB for $P_p \simeq P_c$. Moreover, the response of the resonator at the pump frequency (green line) —measured simultaneously using a voltage meter connected in parallel to the spectrum analyzer— is drawn as well for comparison. The sharp drop in the region $P_p \sim P_c$, coinciding with the amplification of the signal,

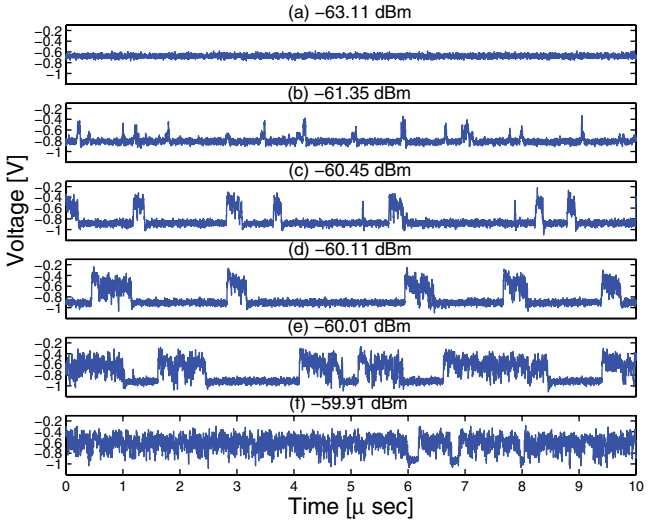

Fig. 6: (Color online) Snapshots of the resonator response measured in the time domain during an IM operation. (a)–(d) display the resonator response at pump powers lower than the critical value. (e) At the critical value. (f) Exceeding the critical value.

indicates that the transmitted pump is depleted and power is transferred to other frequencies.

Figure 5 exhibits a periodic dependence of the signal gain on ϕ_{LO}, having a gain modulation of about 30 dB peak to peak between the amplification and de-amplification quadratures. It is worthwhile mentioning that in this measurement not only the signal shows a periodic dependence on ϕ_{LO} but also the noise floor which exhibits up to 20 dB modulation (measured at $f_p + 1.5\delta$).

Another interesting aspect of this device is revealed by examining its response in the time domain while applying an IM measurement using the homodyne setup shown in fig. 1 (see path (2)). This is achieved by connecting a fast oscilloscope in parallel to the spectrum analyzer at the output. A few representative snapshots of the device behavior measured in the time domain are shown in fig. 6, where each subplot corresponds to a different applied pump power. In subplot (a) the pump power is about 3 dBm lower than the critical value and it displays a constant voltage level. As the pump power is increased (subplot (b)) separated spikes start to emerge. Increasing the power further causes the spikes to start bunching together and as a consequence forming larger groups (subplots (c) and (d)). This bunching process reaches an optimal point at the pump power corresponding to the peak in the IM gain (subplot (e)). Above that value, such as the case in subplot (f), the spikes become saturated and the gain drops.

Such behavior in the time domain reveals also the underlying mechanism responsible for the amplification. As is clear from the measurement traces the rate of spikes strongly depends on P_p at the vicinity of P_c, thus adding a small signal at $f_p + \delta$ (which is effectively equivalent to applying an amplitude modulation of the pump at frequency δ), results in modulation of the rate of spikes at the same frequency, and consequently yields a large response at the signal and the idler tones.

In an attempt to account for the unique temporal response presented in fig. 6, we refer to the two equations of motion governing the dc-SQUID system given by [39]

$$\begin{aligned}\beta_C \frac{\ddot{\delta}_1}{I_c}\left(\frac{\Phi_0}{2\pi R_J}\right)^2 + \dot{\delta}_1\left(\frac{\Phi_0}{2\pi R_J}\right) &= -\frac{\partial U}{\partial \delta_1} + I_{\mathrm{n}1}\\ \beta_C \frac{\ddot{\delta}_2}{I_c}\left(\frac{\Phi_0}{2\pi R_J}\right)^2 + \dot{\delta}_2\left(\frac{\Phi_0}{2\pi R_J}\right) &= -\frac{\partial U}{\partial \delta_2} + I_{\mathrm{n}2},\end{aligned} \tag{1}$$

where Φ_0 is the flux quantum, R_J is the shunt resistance of the junctions, I_c is the critical current of each junction, δ_1, δ_2 are the gauge-invariant phase differences across junctions 1 and 2, respectively, I_{n1}, I_{n2} are equilibrium noise currents generated in the shunt resistors having —in the limit of high temperature— a spectral density of $S_{I_{\mathrm{n}}} = 4k_BT/R_J$, β_C is a dimensionless parameter defined as $\beta_C \equiv 2\pi I_c R_J^2 C_J/\Phi_0$, where C_J is the junction capacitance (herein we solve for the underdamped SQUID case where $\beta_C \gg 1$) and U is the potential energy of the system which reads

$$\begin{aligned}U = &-\frac{I}{2}(\delta_1+\delta_2) + \frac{2I_c}{\pi\beta_L}\left(\frac{\delta_1-\delta_2}{2} - \frac{\pi\Phi}{\Phi_0}\right)^2\\ &-I_c(\cos\delta_1 + \cos\delta_2),\end{aligned} \tag{2}$$

where Φ is the applied magnetic flux, I is the bias current flowing through the dc-SQUID, and β_L is a dimensionless parameter defined as $\beta_L \equiv 2L_sI_c/\Phi_0$. While the circulating current flowing in the dc-SQUID loop is given by $I_{\mathrm{circ}}(t) = I_c(\delta_1 - \delta_2 - 2\pi\Phi/\Phi_0)/\pi\beta_L$.

Furthermore, in order to account for the resonator response as well, we make two simplifying assumptions: 1) We model our resonator as a series RLC tank oscillator characterized by an angular frequency $\omega_0 = 1/\sqrt{LC} = 2\pi \cdot 8.219\,\mathrm{GHz}$, and a characteristic impedance $Z_0 = \sqrt{L/C}$, where L and C are the inductance and the capacitance of the resonant circuit respectively. (2) We neglect the mutual inductance that may exist between the inductor and the dc-SQUID.

Under these simplifying assumptions, one can write the following equation of motion for the charge on the capacitor denoted by $q(t)$:

$$\frac{Z_0\ddot{q}}{\omega_0} + R\dot{q} + \omega_0 Z_0 q + V_{sq} + V_{\mathrm{in}} + V_{\mathrm{n}} = 0, \tag{3}$$

where V_{n} is a voltage noise term having —in the limit of high temperature— a spectral density of $S_{V_{\mathrm{n}}} = 4Rk_BT$, $V_{\mathrm{in}}(t) = \mathrm{Re}\,(V_0 e^{-i\omega_p t})$ is an externally applied sinusoidal voltage oscillating at the pump angular frequency ω_p and having a constant voltage amplitude V_0. Whereas, $V_{sq} = \Phi_0(\dot{\delta}_1 + \dot{\delta}_2)/4\pi$ designates the voltage across the dc SQUID. Using these notations the bias current in eq. (2) reads $I = \dot{q}$.

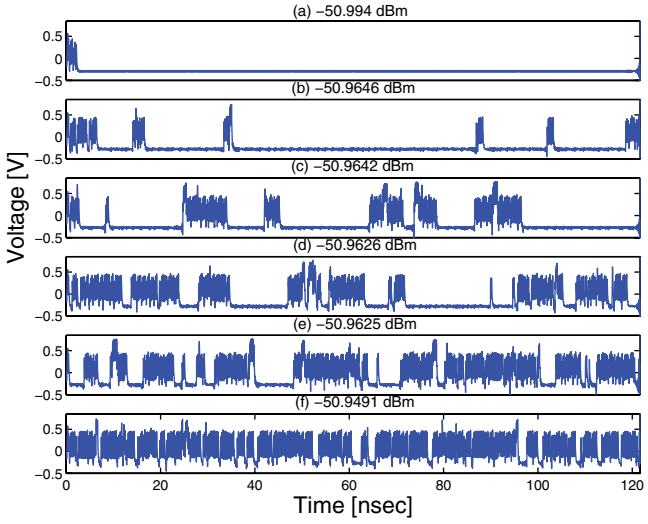

Fig. 7: (Color online) A simulation result. The output field exhibits spikes in the time domain similar to the spikes shown in fig. 6. The spikes occur whenever the system locus jumps from one well to another due to the presence of stochastic noise while driving the system near a critical point. In this simulation run the system was simulated over a period of 1000 time cycles of pump oscillations (one of the constraints set on the simulation was maintaining a reasonable computation time). The parameters that were employed in the simulation (same as experiment) are $\omega_0 = \omega_p = 2\pi \cdot 8.219\,\mathrm{GHz}$, $\beta_L = 3.99$, $R_J = 9.4\,\Omega$, $\Phi = \Phi_0/2$ and $\phi_{LO} = \pi$. The rest of the parameters were set in order to reproduce the measurement result: $\gamma_1 = 10^7\,\mathrm{Hz}$, $R = 3.3\,\Omega$, $\beta_C = 5.86$ and $Z_0 = 10\,\Omega$ (corresponding experimental values are: $\gamma_1 \simeq 2.4 \cdot 10^7\,\mathrm{Hz}$, $Z_0 \simeq 50\,\Omega$, C_J was not measured directly, a capacitance on the order of 0.7 pF was assumed).

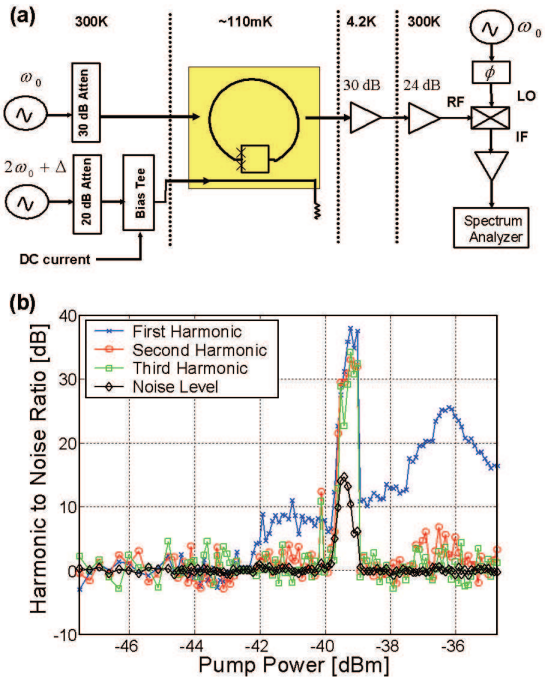

Fig. 8: (Color online) (a) A homodyne setup employed in measuring parametric excitation. Subplot (b) exhibits harmonic-to-noise ratio of the generated three harmonics at $\delta = 5\,\mathrm{kHz}$, 2δ, 3δ, as well as the noise spectral density at 1.5δ as a function of increasing pump power applied at $2f_0 + \delta$. All peaks in the power of the harmonics including the noise rise are measured relative to the noise floor at low pump power. In this measurement a maximum peak of 38 dB is attained at the first harmonic. The signal power applied to the resonator at f_0 is $P_s = -80\,\mathrm{dBm}$, while the external flux is $\Phi \simeq 0.6\Phi_0$.

Finally in order to relate the observed output signal in fig. 6 at the output of the homodyne scheme to the fast oscillating solution q, we first express the charge on the capacitor as $q(t) = \sqrt{2\hbar/Z_0}\mathrm{Re}\,[A(t)e^{-i\omega_p t}]$, where $A(t)$ is a slow envelope function, second, we employ the input-output relation [24], $V_{\mathrm{out}}(t) = V_0 - i\sqrt{32 Z_0 \hbar \gamma_1^2}A(t)$, where γ_1 is the coupling constant between the resonator and the feedline, in order to obtain the field at the output port. Third, we account for the phase shift by evaluating the expression $2V_{LO}\mathrm{Re}\,[V_{\mathrm{out}}(t)e^{i\phi_{LO}}]$, where V_{LO} corresponds to the amplitude of the LO.

By integrating these stochastic coupled equations of motion numerically, while employing device parameters which are relevant for our case, one finds that the observed temporal behavior of the system can be qualitatively explained in terms of noise-induced jumps between different potential wells forming the potential landscape of the dc-SQUID which is given by eq. (2). As a consequence of applying the voltage V_{in} to the integrated system, the potential landscape of the dc-SQUID oscillates at the pump frequency, and its oscillation amplitude grows with the amplitude of the incoming voltage. However, inter-well transitions of the system become most dominant as the oscillation voltage reaches a critical value at which the potential landscape of dc-SQUID becomes tilted enough —due to the current flowing in the system— in order to allow frequent noise-assisted escape events from one well to another or across several wells, which in turn cause a voltage drop to develop across the dc-SQUID and induce jumps in the circulating current. Such hopping of the system state is manifested as well in the homodyne output field response shown in fig. 7, which in a qualitative manner mimics successfully the main temporal features shown in fig. 6.

It is also clear from this inter-well transitions model that the amplification in this case is different from the so-called Josephson Bifurcation Amplifier (JBA) [14], as in the latter case the system is confined to only one well and the bifurcation occurs between two oscillation states having different amplitudes. The extent to which bifurcation amplifiers such as the presently considered one and the JBA are quantum-limited detectors [40,41], is still largely an open problem. As such it will be the subject of a future study [42].

Moreover, just as in the recent experiment by Yamamoto *et al.* [20] we have additionally employed our device as a parametric amplifier. To this end, we have used the parametric excitation scheme exhibited in fig. 8(a) in

which the pump and signal tones are applied to different ports. The main rf signal (pump) is applied to the flux-line at the vicinity of twice the resonance frequency of the resonator $2f_0 + \delta$ ($\delta \equiv \Delta/2\pi = 5\,\mathrm{kHz}$) and $2f_0 = 16.438\,\mathrm{GHz}$ does not coincide with any resonance of the device. Whereas, the signal, being several orders of magnitude lower than the pump, is fed to the resonator port at f_0 and its main purpose is to probe the system response.

In fig. 8(b) we exhibit a parametric excitation measurement result obtained using this device at $\Phi \simeq 0.6\Phi_0$. In this result there is evidence of one of the characteristic fingerprints of a parametric amplifier: the existence of an excitation threshold above which there is a noise rise and an abrupt amplification of the harmonic at δ (which results from a nonlinear frequency mixing at the dc-SQUID). As can be seen in the figure at about $-40\,\mathrm{dBm}$ the first harmonic generated at δ and the two higher-order harmonics at 2δ, 3δ rise abruptly and considerably up to a maximum of 38 dB measured at the first harmonic above the noise floor. Also in a separate measurement result (data not shown) the first harmonic has been found to display $\simeq 20\,\mathrm{dB}$ peak-to-peak modulation as a function of external magnetic field.

In conclusion, in this work we have designed and fabricated a superconducting stripline resonator containing a dc-SQUID. We have shown that this integrated system can serve as a strong sensitive amplifier. We have studied the device using IM measurement and parametric excitation. In both schemes the device exhibited distinct threshold behavior, strong noise rise and large amplification of coherent side-band signals generated due to the nonlinearity of the dc-SQUID. In addition, we have investigated the system response in the time domain during IM measurements. We have found that in the vicinity of the critical input power the system becomes metastable and consequently exhibits noise-activated spikes in the transmitted power. We have shown that this kind of behavior can be explained in terms of noise-assisted hopping of the system state between different potential wells. We have also demonstrated that the main features observed in the time domain can be qualitatively captured by solving the equations of motion for the dc-SQUID in the presence of rf-current bias and stochastic noise. Such a device may be exploited under suitable conditions in a variety of intriguing applications ranging from generating quantum squeezed states to parametric excitation of zero-point fluctuations of the vacuum.

* * *

This work was supported by the Israel Science Foundation, the Deborah Foundation, the Poznanski Foundation, Russel Berrie Nanotechnology Institute, US-Israel Binational Science Foundation and MAFAT. BA was supported by the Ministry of Science, Culture and Sports.

REFERENCES

[1] Nakamura Y. *et al.*, *Nature*, **398** (1999) 786.
[2] Shnirman A. *et al.*, *Phys. Rev. Lett.*, **79** (1997) 2371.
[3] Makhlin Y. *et al.*, *Rev. Mod. Phys.*, **73** (2001) 357.
[4] Bouchiat V. *et al.*, *Phys. Scr.*, **T76** (1998) 165.
[5] Vion D. *et al.*, *Science*, **296** (2002) 886.
[6] Chiorescu I. *et al.*, *Science*, **299** (2003) 1869.
[7] Lupascu A. *et al.*, *Phys. Rev. Lett.*, **93** (2008) 177006.
[8] Wallraff A. *et al.*, *Nature*, **431** (2004) 162.
[9] Martinis J. *et al.*, *Phys. Rev. Lett.*, **89** (2002) 117901.
[10] Yamamato T. *et al.*, *Nature*, **421** (2003) 823.
[11] Claudon J. *et al.*, *Phys. Rev. Lett.*, **93** (2004) 187003.
[12] Zorin A. B., *Phys. Rev. Lett.*, **76** (1996) 4408.
[13] Sillanpaa M. A. *et al.*, *Phys. Rev. Lett.*, **93** (2004) 066805.
[14] Siddiqi I. *et al.*, *Phys. Rev. Lett.*, **93** (2004) 207002.
[15] Schreier J. A. *et al.*, *Phys. Rev. B*, **77** (2008) 180502.
[16] Yurke B. *et al.*, *Phys. Rev. A*, **39** (1989) 2519.
[17] Movshovich R. *et al.*, *Phys. Rev. Lett.*, **65** (1990) 1419.
[18] Yurke B. *et al.*, *IEEE Trans. Magn.*, **25** (1989) 1371.
[19] Spietz L. *et al.*, *Appl. Phys. Lett.*, **93** (2008) 082506.
[20] Yamamoto T. *et al.*, *Appl. Phys. Lett.*, **93** (2008) 042510.
[21] Castellanos-Beltran M. A. and Lehnert K. W., *Appl. Phys. Lett.*, **91** (2007) 83509.
[22] Houck A. A. *et al.*, *Nature*, **449** (2007) 328.
[23] Hofheinz M. *et al.*, *Nature*, **454** (2008) 310.
[24] Yurke B. and Buks E., *J. Lightwave Technol.*, **24** (2006) 5054.
[25] Castellanos-Beltran M. A. *et al.*, *Nat. Phys.*, **4** (2008) 929.
[26] Barton G. *et al.*, *J. Opt. B: Quantum Semiclass. Opt.*, **7** (2005) S1.
[27] Dodonov V. V., *Adv. Chem. Phys.*, **119** (2001) 309.
[28] Segev E. *et al.*, *Phys. Lett. A*, **370** (2007) 202.
[29] Dodonov A. V. *et al.*, quant-ph/0806.4035 (2008).
[30] Sandberg M. *et al.*, *Appl. Phys. Lett.*, **92** (2008) 203501.
[31] Laloy A. P. *et al.*, *J. Low Temp. Phys.*, **151** (2008) 1034.
[32] Nation P. D. *et al.*, *Phys. Rev. B*, **78** (2008) 104516.
[33] Fulton T. A. and Dolan G. J., *Phys. Rev. Lett.*, **59** (1987) 109.
[34] Dahm T. and Scalapino D. J., *J. Appl. Phys.*, **81** (1997) 2002.
[35] Chen C. C. *et al.*, *Phys. Rev. B.*, **45** (1992) 4788.
[36] Monaco R. *et al.*, *J. Appl. Phys.*, **88** (2000) 2898.
[37] Abdo B. *et al.*, *Appl. Phys. Lett.*, **88** (2006) 22508.
[38] Tholen E. A. *et al.*, *Appl. Phys. Lett.*, **90** (2007) 253509.
[39] Koch R. H. *et al.*, *Appl. Phys. Lett.*, **38** (1981) 380.
[40] Nakano H. *et al.*, cond-mat/0808.1798v1 (2008).
[41] Dykman M. I., cond-mat/0810.5016v1 (2008).
[42] Blencowe M. P. *et al.*, in preparation.